Science
AAAS

Developmentally Regulated piRNA Clusters Implicate MILI in Transposon Control

Alexei A. Aravin, *et al.*

Science **316**, 744 (2007);
DOI: 10.1126/science.1142612

in fish populations. Selection may therefore favor the retention of many larvae, especially if the probability of encountering better adult habitat by dispersing is low (*15*) or advantages accrue through local adaptation (*16*). A number of mechanisms may be used by larvae to avoid being swept away from natal reefs. Field evidence suggests that reef fish larvae migrate vertically in the water column to exploit currents at different depths and thereby avoid dispersal away from spawning locations (*17*). Larvae are also capable of sustained directional swimming soon after hatching (*18*), and possess a range of well-developed sensory systems to locate and orient to reefs, including sight, smell, and sound (*18*–*21*).

Despite the high levels of self-recruitment we detected, ~40% of juveniles of both species came from outside the MPA. The reef nearest to Kimbe Island is 10 km away, and reefs in this region are typically separated by 5 to 20 km. Ecologically important larval exchange must occur between populations at these scales. Thus, the Kimbe Island MPA is likely to be self-sustaining as well as providing recruitment subsidies to populations beyond its boundaries. Although levels of retention and connectivity may differ where reefs are closer and populations are less isolated, the Kimbe Island example sets a new boundary condition for the scale at which self-recruitment can occur.

Ideally, the size and spacing of marine reserves should be predicated on an understanding of larval dispersal distances (*3*–*6*, *22*). The optimal design should be one in which individual MPAs are large enough so that populations within reserves can sustain themselves, yet small enough and spaced so that a proportion of larvae produced inside the MPA is exported to unprotected areas (*3*, *5*, *12*). Our study suggests that the spatial scale at which coral reef MPAs can achieve these dual goals may be relatively small. However, if natal homing and larval retention are common, some MPAs may fail to deliver substantial recruitment subsidies to locations beyond their boundaries. We therefore support recent suggestions (*23*, *24*) that MPA networks should be combined with conventional management strategies to both protect threatened species and ensure the sustainability of fisheries on coral reefs.

References and Notes

1. E. Sala *et al.*, *Science* **298**, 1991 (2002).
2. F. R. Gell, C. M. Roberts, *Trends Ecol. Evol.* **18**, 448 (2003).
3. B. S. Halpern, R. R. Warner, *Proc. R. Soc. London Ser. B* **270**, 1871 (2003).
4. L. W. Botsford, A. Hastings, S. D. Gaines, *Ecol. Lett.* **4**, 144 (2001).
5. A. L. Shanks, B. A. Grantham, M. H. Carr, *Ecol. Appl.* **13**, S159 (2003).
6. S. R. Palumbi, *Ecol. Appl.* **13**, S146 (2003).
7. P. F. Sale *et al.*, *Trends Ecol. Evol.* **20**, 74 (2005).
8. R. R. Warner, R. K. Cowen, *Bull. Mar. Sci.* **70**, 245 (2002).
9. S. R. Thorrold *et al.*, *Bull. Mar. Sci.* **70**, 291 (2002).
10. S. R. Thorrold, G. P. Jones, S. Planes, J. A. Hare, *Can. J. Fish. Aquat. Sci.* **63**, 1193 (2006).
11. S. E. Swearer *et al.*, *Bull. Mar. Sci.* **70**, 251 (2002).
12. G. P. Jones, S. Planes, S. R. Thorrold, *Curr. Biol.* **15**, 1314 (2005).
13. G. P. Jones, M. J. Milicich, M. J. Emslie, C. Lunow, *Nature* **402**, 802 (1999).
14. R. K. Cowen, C. B. Paris, A. Srinivasan, *Science* **311**, 522 (2006).
15. R. R. Strathmann *et al.*, *Bull. Mar. Sci.* **70**, 377 (2002).
16. D. O. Conover, L. M. Clarke, S. B. Munch, G. N. Wagner, *J. Fish Biol.* **69**, 21 (2006).
17. C. B. Paris, R. K. Cowen, *Limnol. Oceanogr.* **49**, 1964 (2004).
18. J. M. Leis, *Adv. Mar. Biol.* **51**, 57 (2006).
19. G. Gerlach, J. Atema, M. J. Kingsford, K. P. Black, V. Miller-Sims, *Proc. Natl. Acad. Sci. U.S.A.* **104**, 858 (2007).
20. D. Lecchini, J. Shima, B. Banaigs, R. Galzin, *Oecologia* **143**, 326 (2005).
21. S. D. Simpson, M. Meekan, J. Montgomery, R. McCauley, A. Jeffs, *Science* **308**, 221 (2005).
22. L. W. Botsford, F. Micheli, A. Hastings, *Ecol. Appl.* **13**, S25 (2003).
23. R. Hilborn, F. Micheli, G. A. De Leo, *Can. J. Fish. Aquat. Sci.* **63**, 642 (2006).
24. L. W. Botsford, *Bull. Mar. Sci.* **76**, 245 (2005).

25. We thank S. Sheppard of The Nature Conservancy for satellite imagery analyses; E. Laman-Trip for aging juvenile butterflyfish; J. Almany, D. DeVere, N. Gardiner, V. Messmer, M. Srinivasan, C. Syms, and H. Walsh for field and lab assistance; and the Global Environmental Fund, Connectivity Working Group, for providing a forum for discussing different approaches to evaluating marine connectivity. This project was financially supported by an Australian Research Council (ARC) Discovery Grant (DP0208120), the ARC Centre of Excellence for Coral Reef Studies, a Coral Reef Initiative for the South Pacific grant, and NSF through an International Research Fellowship to G.R.A. and grants OCE-0215905 and OCE-0424688.

Supporting Online Material

www.sciencemag.org/cgi/content/full/316/5825/742/DC1
Materials and Methods
References

30 January 2007; accepted 2 April 2007
10.1126/science.1140597

Developmentally Regulated piRNA Clusters Implicate MILI in Transposon Control

Alexei A. Aravin, Ravi Sachidanandam, Angelique Girard, Katalin Fejes-Toth, Gregory J. Hannon*

Nearly half of the mammalian genome is composed of repeated sequences. In *Drosophila*, Piwi proteins exert control over transposons. However, mammalian Piwi proteins, MIWI and MILI, partner with Piwi-interacting RNAs (piRNAs) that are depleted of repeat sequences, which raises questions about a role for mammalian Piwi's in transposon control. A search for murine small RNAs that might program Piwi proteins for transposon suppression revealed developmentally regulated piRNA loci, some of which resemble transposon master control loci of *Drosophila*. We also find evidence of an adaptive amplification loop in which MILI catalyzes the formation of piRNA 5′ ends. *Mili* mutants derepress LINE-1 (L1) and intracisternal A particle and lose DNA methylation of L1 elements, demonstrating an evolutionarily conserved role for PIWI proteins in transposon suppression.

Known piRNAs are not expressed until spermatocytes first enter mid-prophase (pachytene stage) at ~14 days after birth (P14) (*1*–*4*). However, *Mili* expression begins in primordial germ cells at embryonic day 12.5 (*5*, *6*), and transposons, such as L1, can be expressed in both premeiotic and meiotic germ cells (*7*, *8*). We therefore probed a connection between *Mili* and transposon control by examining MILI-bound small RNAs in early-stage spermatocytes. Notably, MILI-associated RNAs could be detected at all developmental time points tested (Fig. 1 and fig. S1). Northern blotting revealed that pre-pachytene piRNAs join MILI before pachytene piRNAs become expressed at P14 (Fig. 1B). The appearance of pre-pachytene piRNAs was MILI-dependent, suggesting a requirement for this protein in either their biogenesis or stability (Fig. 1C). These results raised the possibility that MILI might be programmed by distinct piRNA populations at different stages of germ cell development.

To characterize pre-pachytene piRNAs, we isolated MILI complexes from P10 testes and deeply sequenced their constituent small RNAs. Like pachytene populations, pre-pachytene piRNAs were quite diverse, with 84% being cloned only once. The majority of both pre-pachytene (66.8%) and pachytene (82.9%) piRNAs map to single genomic locations. However, a substantial fraction (20.1%) of pre-pachytene piRNAs had more than 10 genomic matches, as compared to 1.6% for pachytene piRNAs.

Annotation of pre-pachytene piRNAs revealed three major classes (Fig. 2A). The largest (35%) corresponded to repeats, with most matching short interspersed elements (SINEs) (49%), long interspersed elements (LINEs) (15.8%), and long terminal repeat (LTR) retrotransposons (33.8%). Although pachytene piRNAs also match repeats (17%), the majority (>80%) map

Watson School of Biological Sciences, Cold Spring Harbor Laboratory, Howard Hughes Medical Institute (HHMI), 1 Bungtown Road, Cold Spring Harbor, NY 11724, USA.

*To whom correspondence should be addressed. E-mail: hannon@cshl.edu

uniquely in the genome, with only 1.8% mapping more than 1000 times (fig. S2). In contrast, 22% of repeat-derived pre-pachytene piRNAs map more than 1000 times and correspond closely to consensus sequences for SINE B1, LINE L1, and IAP retrotransposons (fig. S2). A second abundant class of pre-pachytene piRNAs (29%) matched genic sequences, including both exons (22%) and introns (7%). A third class matched sequences without any annotation (28%). All three major classes shared signature piRNA characteristics, including a preference for a uridine (U) at their 5′ end (>80%) (Fig. 2A).

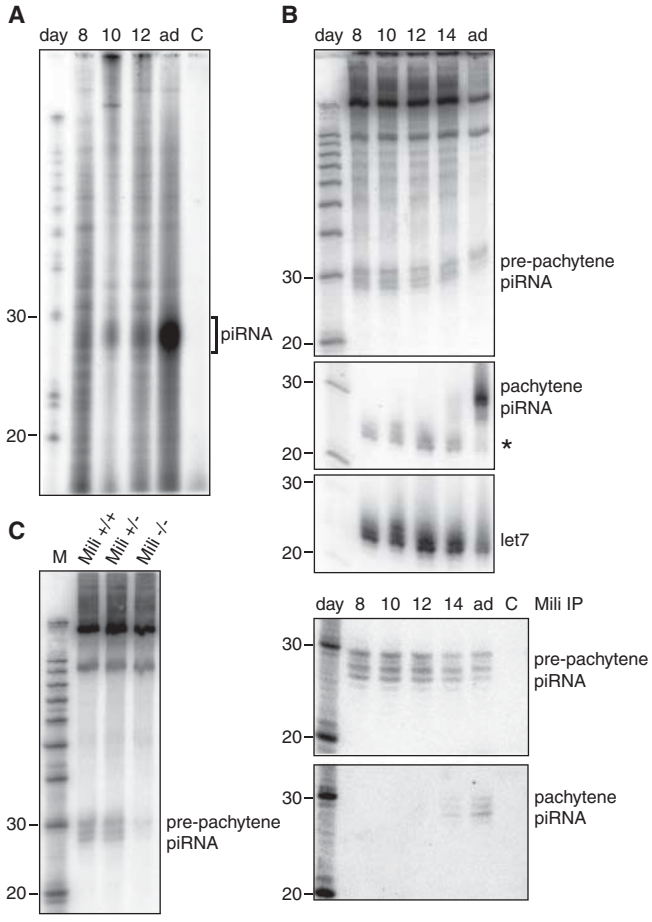

Fig. 1. MILI associates with distinct small RNA populations during spermatogenesis. (**A**) MILI-associated RNAs were analyzed from testes of 8-, 10-, and 12-day-old and adult (ad) mice. C, control immunoprecipitation. (**B**) Testes RNA (three top panels) or RNA from MILI immunoprecipitates (IP) (two bottom panels) from mice of indicated ages was analyzed by Northern blotting for a pre-pachytene piRNA, a pachytene piRNA, or let-7. The asterisk indicates the residual let-7 signal. (**C**) Northern hybridization of RNA isolated from P10 testes of WT mice and *Mili*-heterozygous and *Mili*-homozygous mutants, as indicated. The probe is as in (B). M, RNA size markers.

Pachytene piRNAs derive from relatively few extended genomic regions, with hundreds to thousands of different species encoded from a single genomic strand (*1*, *3*, *4*). Cluster analysis of pre-pachytene piRNAs yielded 909 loci, covering ~0.2% of the mouse genome (5.3 megabases; table S1). Pachytene and pre-pachytene clusters show little overlap (Fig. 2, B and C, and table S1). Overall, pachytene clusters were larger, and each produced a greater fraction of the piRNA population than early clusters, which average 5.8 kb in size (Fig. 2B). Only 56.5% of uniquely mapped pre-pachytene piRNAs can be attributed to clusters, as compared to 95.5% in pachytene piRNA populations. Considered together, these results demonstrate that pre-pachytene and pachytene piRNAs are derived from different genomic locations, with pre-pachytene piRNAs being produced from a broader set of loci.

We were unable to intuit the functional importance of those pre-pachytene clusters that correspond solely to unannotated regions of the genome. The 28% of pre-pachytene piRNAs that correspond to protein coding genes were concentrated in 3′ untranslated regions (3′UTRs) (fig. S3) and showed a strong bias for certain loci, with 8% of the total coming from only 10 genes. However, these were invariably derived from the sense strand, implying that these piRNAs would

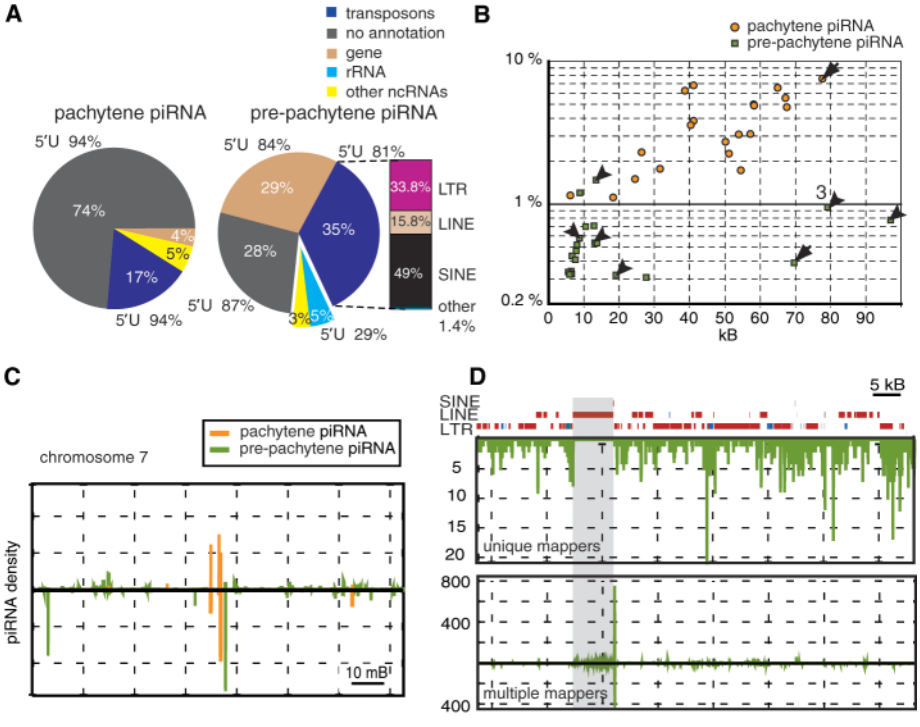

Fig. 2. Characteristics of pachytene and pre-pachytene piRNAs. (**A**) Genomic annotation of piRNA populations and the fraction of sequences with a 5′ U are indicated. rRNA, ribosomal RNA; ncRNA, noncoding RNA. (**B**) The top 20 pachytene and pre-pachytene piRNA clusters are displayed according to the fraction of uniquely mapped piRNAs produced (*y* axis) and cluster sizes (*x* axis). The cluster on chromosome 17, expressed at both stages, is marked with an arrow. Pre-pachytene clusters, enriched in repeat-derived piRNAs, are marked with arrowheads. (**C**) The density of uniquely mapped piRNAs on chromosome 7 is plotted for the plus and minus genomic strands (above and below the axis, respectively). (**D**) Transposable element fragments and piRNA density are plotted for a repeat-rich pre-pachytene piRNA cluster ["3" in (B)]. Elements, separated by type, are indicated as red boxes on the plus strand and as blue boxes on the minus strand. Gray shadowing indicates LINE and adjacent SINE fragments that closely match their consensus.

be unable to direct posttranscriptional gene silencing. Using semiquantitative reverse transcription polymerase chain reaction (RT-PCR), we were unable to detect differences in the expression of genes corresponding to piRNA clusters by comparing wild-type (WT) to *Mili*-mutant animals. We do not yet understand what distinguishes genes that contribute piRNAs but do note that at least some have repetitive elements resident in their 3′UTRs (fig. S3).

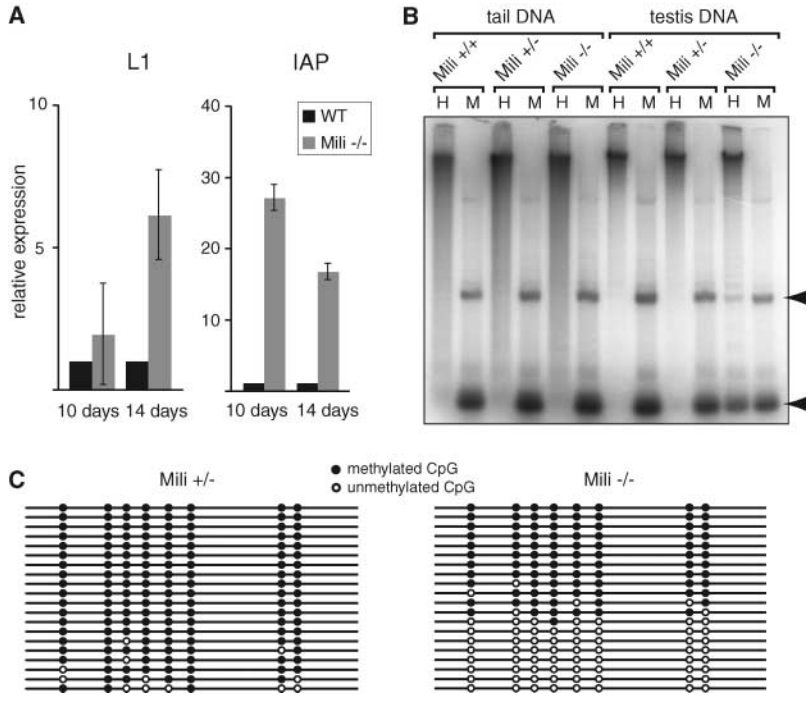

Fig. 3. *Mili* regulates L1 and IAP elements. (**A**) Quantitative RT-PCR for IAP and L1 expression in testes from WT or *Mili*-null mice, as indicated. Expression was assessed at P10 and P14. Error bars indicate SD. (**B**) DNA was isolated from the tails or testes of $Mili^{+/+}$, $Mili^{+/-}$, or $Mili^{-/-}$ animals; digested with either a methylation-insensitive [Msp I (M)] or a methylation-sensitive [Hpa II (H)] restriction enzyme; and used in a Southern blot with a probe from the LINE-1 5′UTR. Arrowheads indicate bands arising from loss of methylation in the Mili-null animals. (**C**) Bisulfite sequencing of the first 150 bases of a specific L1 element was done in $Mili^{+/-}$ or $Mili^{-/-}$ animals.

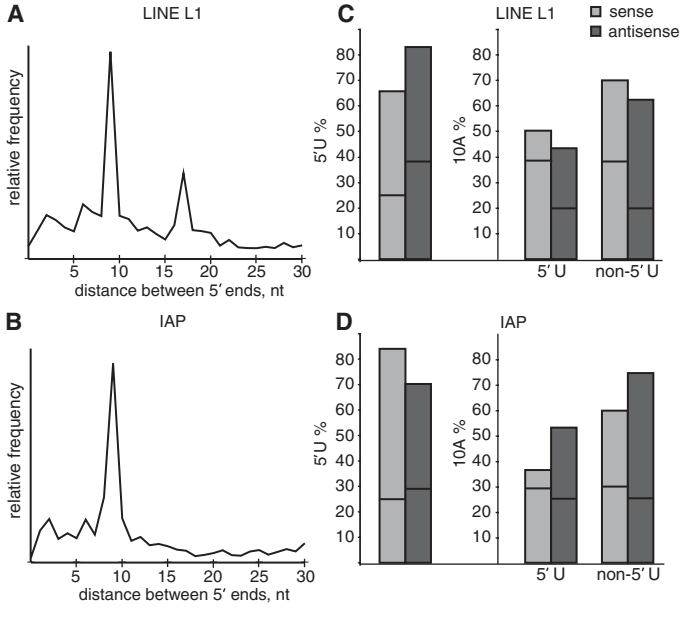

Fig. 4. A Piwi-mediated piRNA amplification loop in mammals. L1 (**A**) and IAP (**B**) piRNAs were aligned to their consensus sequences allowing up to three mismatches, and distances separating 5′ ends of complementary piRNA were plotted. nt, nucleotide. Nucleotide biases were calculated for L1 (**C**) and IAP (**D**) piRNAs analyzed in (A) and (B). The fraction of A at position 10 was plotted both for piRNA classes that contain and lack a 5′ U. For each bar, the percentage of U or A residues that would be expected by random sampling is indicated by a solid line across the bar.

Clusters that are rich in transposon sequences were among the most prominent, as judged by either their size or the number of piRNAs that they generate. Two of these were the largest prepachytene clusters (97 and 79 kb, respectively). Although uniquely mapping piRNAs were derived largely from one genomic strand, the mixed orientations of transposable elements within clusters led to the production of both sense and antisense piRNAs. As is observed in *Drosophila*, repeat-rich mouse piRNA clusters typically contained multiple element types, many of which comprise damaged or fragmented copies (*9*). In many repeat-rich clusters, the orientation of most elements was similar. For example, similarly oriented elements in the two longest clusters (Fig. 2D and table S1) resulted in the production of mainly antisense piRNAs, similar to the *flamenco* piRNA locus in *Drosophila* (*9*, *10*).

We examined the possibility that prepachytene piRNAs might program MILI to repress transposon activity. *Mili* mutation showed substantial effects on L1 and IAP expression, with each increasing its levels by a factor of at least 5 to 10 (Fig. 3A). These studies were carried out at P10 and P14, before an overt *Mili* phenotype becomes apparent.

Although posttranscriptional mechanisms likely contribute to silencing, CpG methylation is critical for transposon repression in mammals (*11*–*16*). Both analysis with methylation-sensitive restriction enzymes and bisulfite DNA sequencing revealed substantial demethylation of L1 elements in *Mili*-mutant testes (Fig. 3, B and C). In the latter case, the ~50% of L1 sequences that remain methylated in the mutant are likely derived from the somatic compartment. Considered together, our data suggest that pre-pachytene piRNAs might help to guide methylation of L1 elements, although we cannot distinguish between roles in de novo versus maintenance methylation.

In *Drosophila*, Piwi-mediated cleavage promotes the formation of secondary piRNAs (*9*, *17*). This allows active transposons and piRNA clusters to participate in a feed-forward loop that both degrades transposon mRNAs and amplifies silencing (*9*). The presence of both sense and antisense piRNAs from mammalian transposable elements creates the potential for engagement of a similar amplification cycle. This cycle creates two tell-tale features. First, because Piwi proteins cleave targets opposite nucleotides 10 and 11 of the guide, piRNAs generated within the loop overlap their partners by precisely 10 nucleotides (*9*, *17*). As predicted, we observed enrichment for piRNAs corresponding to L1 and IAP retrotransposons, in which the 5′ ends of sense and antisense partners are separated by precisely 10 nucleotides (Fig. 4, A and B). Second, because most piRNAs begin with a U, piRNAs produced by Piwi-mediated cleavage are enriched for adenine (A) at position 10 (*9*, *17*). This bias was prevalent in L1- and IAP-derived piRNAs [the fraction of A at position 10 (10A) in

Fig. 4, C and D]. For piRNAs to be cleavage-competent and active in the amplification cycle, they must retain a high degree of complementarity to their targets (fig. S4). Consistent with this hypothesis, piRNAs that map uniquely in the genome have a lower bias for 10A (e.g., 38.7% for non-5′U piRNAs matching LTR-containing retrotransposons) than do piRNAs with many (e.g., >1000) genomic matches (61.5%).

Our results suggest a conserved pathway through which a developmentally regulated cascade of piRNA clusters programs Piwi proteins to repress transposons in mammals. One key difference between transposon control in *Drosophila* and mammals is the role of cytosine methylation in maintaining stable repression. In plants, it is well established that small RNAs can guide methylation of complementary sequences (*18*, *19*). The observations that *Miwi2* (*20*) and *Mili* mutations strongly affect methylation of L1 elements and that MILI binds L1-targeted small RNAs suggest that mammals may also harbor an RNA-dependent DNA methylation pathway.

References and Notes

1. N. C. Lau *et al.*, *Science* **313**, 363 (2006).
2. S. T. Grivna, E. Beyret, Z. Wang, H. Lin, *Genes Dev.* **20**, 1709 (2006).
3. A. Aravin *et al.*, *Nature* **442**, 203 (2006).
4. A. Girard, R. Sachidanandam, G. J. Hannon, M. A. Carmell, *Nature* **442**, 199 (2006).
5. S. Kuramochi-Miyagawa *et al.*, *Mech. Dev.* **108**, 121 (2001).
6. S. Kuramochi-Miyagawa *et al.*, *Development* **131**, 839 (2004).
7. H. H. Kazazian Jr., *Science* **303**, 1626 (2004).
8. D. Branciforte, S. L. Martin, *Mol. Cell. Biol.* **14**, 2584 (1994).
9. J. Brennecke *et al.*, *Cell* **128**, 1089 (2007).
10. A. Bucheton, *Trends Genet.* **11**, 349 (1995).
11. G. Liang *et al.*, *Mol. Cell Biol.* **22**, 480 (2002).
12. F. Gaudet *et al.*, *Mol. Cell Biol.* **24**, 1640 (2004).
13. Z. Lippman, B. May, C. Yordan, T. Singer, R. Martienssen, *PLoS Biol.* **1**, E67 (2003).
14. D. Bourc'his, T. H. Bestor, *Nature* **431**, 96 (2004).
15. J. A. Yoder, C. P. Walsh, T. H. Bestor, *Trends Genet.* **13**, 335 (1997).
16. T. H. Bestor, D. Bourc'his, *Cold Spring Harbor Symp. Quant. Biol.* **69**, 381 (2004).
17. L. S. Gunawardane *et al.*, *Science* **315**, 1587 (2007).
18. W. Aufsatz, M. F. Mette, J. van der Winden, A. J. Matzke, M. Matzke, *Proc. Natl. Acad. Sci. U.S.A.* **99** (suppl. 4), 16499 (2002).
19. O. Mathieu, J. Bender, *J. Cell Sci.* **117**, 4881 (2004).
20. M. A. Carmell *et al.*, *Dev. Cell* **12**, 503 (2007).

21. piRNA sequences are available in the Gene Expression Omnibus (GEO) database (accession # GSE7414). We thank H. Lin (Yale University) for the *Mili* knockout mouse. A.A.A. is supported by a Cold Spring Harbor Laboratory Association fellowship. A.G. is a Florence Gould Fellow of the Watson School of Biological Sciences. G.J.H. is an HHMI investigator. This work was supported by grants from NIH and from Katherine W. Davis (G.J.H.).

Supporting Online Material

www.sciencemag.org/cgi/content/full/1142612/DC1
Materials and Methods
Figs. S1 to S4
Table S1
References

16 March 2007; accepted 30 March 2007
Published online 19 April 2007;
10.1126/science.1142612
Include this information when citing this paper.

Protein Dynamics Control the Kinetics of Initial Electron Transfer in Photosynthesis

Haiyu Wang,[1,2] Su Lin,[1,2] James P. Allen,[2] JoAnn C. Williams,[2] Sean Blankert,[1,2] Christa Laser,[1,2] Neal W. Woodbury[1,2]*

The initial electron transfer dynamics during photosynthesis have been studied in *Rhodobacter sphaeroides* reaction centers from wild type and 14 mutants in which the driving force and the kinetics of charge separation vary over a broad range. Surprisingly, the protein relaxation kinetics, as measured by tryptophan absorbance changes, are invariant in these mutants. By applying a reaction-diffusion model, we can fit the complex electron transfer kinetics of each mutant quantitatively, varying only the driving force. These results indicate that initial photosynthetic charge separation is limited by protein dynamics rather than by a static electron transfer barrier.

Solar energy conversion in photosynthesis involves electron transfer between an excited donor molecule and a neighboring acceptor molecule that are embedded in the reaction center, an intrinsic membrane protein-pigment complex. In the photosynthetic reaction centers of *Rhodobacter sphaeroides*, an excited electron donor, P* (P is a pair of bacteriochlorophylls) transfers an electron in picoseconds to a neighboring bacteriochlorophyll, B_A, and subsequently to a bacteriopheophytin, H_A (Fig. 1). The state $P^+H_A^-$ exists for about 200 ps before the electron is transferred to a quinone Q_A (*1*–*3*). One aspect of reaction center function that is challenging to understand quantitatively is the dependence of the initial charge separation kinetics on driving force (the free energy difference between P* and the initial charge-separated state). Many mutants with altered standard free energies for the initial charge separation have been studied, and in general the dependence of the electron transfer rate on driving force is not consistent with the weak temperature dependence of this reaction (*4*–*6*). Additionally, the kinetics of the charge separation are complex, requiring multiple decay components for an accurate description in both wild-type and mutant reaction centers (*4*–*8*). Many different kinetic models have been developed to explain these features on the basis of vibrational nonequilibrium (*9*–*11*), static inhomogeneity (*4*, *7*, *12*), and multiple interacting states (*8*, *13*). However, none of these quantitatively predicts the complex reaction center kinetics as a function of driving force.

The protein environment of the reaction center represents an inhomogeneous solvent, which relaxes upon excitation and charge separation over many different time scales (*11*, *14*–*16*). Thus, a complete model of electron transfer must take into account protein motion, a concept suggested previously by Chandler and co-workers on the basis of molecular dynamics simulations (*15*). Molecular dynamics simulations modeling the electron transfer reaction, as pioneered by Warshel and Parson (*11*, *14*), suggest that the energy fluctuations between states due to protein movement are correlated with initial electron transfer kinetics.

The structure-based theoretical treatments described above give detailed mechanistic information but are challenging to apply directly to the analysis of experimental data. Fortunately, simplified models have been developed to describe electron transfer between small molecules in viscous solvents, resulting in the reduction of the solvent motion to one or two generalized dimensions (*17*–*19*). One way to represent such a reaction is to divide the solvent response (the solvent reorganization) into two dimensions: the instantaneous response of the solvent (much faster than electron transfer) and the slower, longer-range solvent reorganization that occurs on the time scale of electron transfer and longer. For this situation, the kinetic time course can be described by the reaction-diffusion equation (*19*)

$$\frac{\partial \rho(x,t)}{\partial t} = [\hat{L} - K(x)]\rho(x,t) \qquad (1)$$

Here, $\rho(x,t)$ is the distribution of the initial electron donor state (P*) along a reaction coordinate, x, as a function of time, t. The reaction coordinate x is associated with the motion of the solvent (protein) on the time scale of the electron transfer. $K(x)$ is the rate constant for electron transfer at the reaction coordinate position x (*20*):

$$K(x) = \frac{J^2}{\hbar}\sqrt{\frac{\pi}{\lambda_f k_B T}}\exp\left[-\frac{(\Delta G^0 + \lambda - 2x\sqrt{\lambda_p})^2}{4\lambda_f k_B T}\right] \qquad (2)$$

where J is the electronic coupling matrix element; ΔG^0 is the standard free energy difference between the reactants and the products; λ is the total

[1]Biodesign Institute, Arizona State University, 1001 South McAllister Avenue, Tempe, AZ 85287–5201, USA. [2]Department of Chemistry and Biochemistry, Arizona State University, Tempe, AZ 85287–1604, USA.

*To whom correspondence should be addressed. E-mail: Nwoodbury@asu.edu